Extended Injectant Mole-Fraction Imaging of Supersonic Mixing using Acetone PLIF

Hidemi TAKAHASHI,[*] Shuzo IKEGAMI,[*] Mitsutomo HIROTA,[**] and Goro MASUYA[*]
[*]Department of Aerospace Engineering, Tohoku University
6-6-01 Aramaki-Aza-Aoba, Aoba-ku, Sendai, Miyagi 980-8579, Japan
[**]Department of Mechanical Systems Engineering, Muroran Institute of Technology
27-1 Mizumoto-cho, Muroran, Hokkaido 050-8585, Japan
takahashi.h@scrj.mech.tohoku.ac.jp

Keywords: Acetone PLIF, Fluorescence ratio method, Scramjet

Abstract

The fluorescence ratio method for processing planar laser induced fluorescence (PLIF) data was generalized for quantitative imaging of the injectant mole-fraction in supersonic mixing flowfields. The original fluorescence ratio approach was introduced by Hartfield et al. for tests in a special closed-loop wind tunnel to eliminate the effects of thermodynamic property variations in compressible flowfields and to provide a quantitative means of mole-fraction measurement. However, they implicitly assumed that the tracer molecules were seeded at the same fraction in both main and secondary flows. In the present study, we proposed generalizing the Hartfield method by considering differences in the tracer seeding rates. We examined the generalized method in a mixing flowfield formed by sonic transverse injection into a Mach 1.8 supersonic air stream. The injectant mole-fraction distribution obtained from PLIF data processed by our new approach showed better agreement with the gas chromatograph than one based on the Hartfield method.

Introduction

Scramjet is one of the most promising candidates for hypersonic vehicles and air-breathing space planes. In this speed range, combustion is likely to be limited by fuel mixing due to the compressibility effect or small difference in velocity between fuel and air. One of the key technologies for designing a successful scramjet engine is the enhancement of mixing between fuel and air to provide high combustion efficiency. Many concepts for supersonic mixing enhancement have been proposed and experimentally validated by a number of investigators.[1)]

Planar laser induced fluorescence with acetone tracer (acetone PLIF) was developed to investigate gas concentration in non-reacting compressible flows because of its excellent spatial and temporal resolution, strong fluorescence signal, and non-intrusiveness, and because the tracer is less harmful to the human body and to the facility.[2)]

Since the fluorescence signal depends upon not only the mole-fraction of tracer gas but also the local thermodynamic properties, an image taken by PLIF cannot be directly related to the degree of mixing.

A fluorescence signal ratio approach introduced by Hartfield et al.[3-8)] is quite useful in enabling us to eliminate thermodynamic dependencies, thus providing a quantitative means of mole-fraction measurement. Once planar mole-fraction distributions are obtained in sufficient numbers, the injectant mole-fraction in any desired plane in the flowfield can be easily obtained. The principle of the fluorescence ratio method is to take the ratio of two images recorded in two different seeding conditions: one for tracer seeded only into the jet flow and the other for tracer seeded into both the jet and the main flow. This idea makes it possible to cancel the thermodynamic dependencies as well as any non-uniformity in the collection optics. Though it is a very attractive technique, it is not clear whether or not this approach is applicable to configurations other than theirs, as their experiments were conducted using a closed-loop wind tunnel where the tracer seeding levels of both flows were kept constant and equal during the whole experimental period.

In the present work, we generalize the Hartfield fluorescence ratio method so as to apply it to other experimental setups. The generalized fluorescence ratio method is verified by comparing the injectant mole-fraction distribution obtained by acetone PLIF to a distribution obtained by gas chromatography.

Experimental Arrangements and Conditions

Wind tunnel and Test section

A schematic diagram of the present experimental apparatus is displayed in Fig. 1. A suction-type supersonic wind tunnel was used. Unheated atmospheric air was inhaled into a vacuum tank through a rectification section, a two-dimensional contoured nozzle of nominal Mach number 1.8, and a test section. The vacuum tank had a volume of 8 m^3 and was evacuated to about 5 kPa before each test run. The rectification section was an acrylic rectangular duct 100 mm wide, 100 mm high, and 400 mm long. A perforated plate was attached at the end of the rectification section to enhance mixing of ambient inhaled air and acetone-seeded pressurized air. Five sheets of meshes and a bundle of straws used for rectification of air/acetone mixture gas were set inside in the middle of this section. Compressed dry air from an air bomb was introduced into a bubbling container to vaporize the acetone and was then fed to the tracer gas injectors to seed acetone molecules as a tracer for LIF measurements in the main airstream. There was another similar feeding line for acetone-air mixture

that was directly connected to an injection port on the test section. The mole-fraction of seeded acetone was assumed to be well below a saturated condition at room temperature; the details of this will be discussed below. The test section was a rectangular duct 30 mm wide, 30 mm high, and 200 mm long. A sonic transverse injector 2.5 mm in diameter was located on the centerline of the tunnel wall. Quartz glass windows were set on the three walls for optical access, enabling LIF measurements.

In this paper, the following Cartesian coordinate system is used. The origin is located at the center of the injector orifice. The streamwise axis is *x*, the transverse axis *y*, and the spanwise axis *z*.

PLIF measurement

The light source used for inducing acetone fluorescence was fourth-harmonic radiation from a Q-switched pulsed Nd:YAG laser with a wavelength of 266 nm and energy of 70 mJ/pulse, with a maximum repetition rate of 10 Hz. The laser beam was expanded into a two-dimensional sheet 30 mm wide and 0.5 mm thick. This was used by six mirrors, two positive cylindrical lenses (f = 200 mm), and one negative cylindrical lens (f = - 20 mm) so that the flowfield could be measured with parallel light. Given these laser sheet characteristics, the pulse energy of 70 mJ was well below the saturation level for acetone fluorescence. Mirrors were used to orient the sheet in the streamwise vertical (*x*-*y*) and spanwise vertical (*y*-*z*) planes.

The fluorescence images were recorded using a digital charge-coupled device (CCD) camera system with an image intensifier unit and a micro-Nikko 50 mm, *f*/2.8 lens. Operation of these devices was synchronized by a pulse generator. A band-pass filter (passband 390 ± 100 nm) was attached in front of the camera lens to block stray light. MATLAB 7.1 was used as post-processing software.

Gas sampling measurement

Figure 2 illustrates the test section used for the gas sampling experiments. It had the same cross section as the one used for the LIF measurement but was 130 mm longer. All of the walls except for the injector wall were made of clear acrylic resin. A three-point gas sampling probe rake was inserted through a port on the wall opposite to the injector wall. The probe rake could be moved in the *x*-direction from 5 to 30 mm at intervals of 5 mm and in the *y*-direction from 3.0 to 14.0 mm. Each sampling probe had an outer diameter of 0.88 mm and an inner diameter of 0.58 mm at the tip. The distance between the probes was approximately 3.0 mm. The blockage ratio of the probe rake parts to the tunnel cross section was 0.34 %, which is an acceptable value for avoiding an unstart of the wind tunnel. The injector diameter D was 2.8 mm in this experiment. The diameter of the gas sampling test section was different from that in the LIF measurement due to an inaccuracy in manufacturing. Therefore, we treated all the length scales from the injector orifice as a length non-dimensionalized by each diameter to cancel out any effects resulting from the difference in diameter. The line scavenging and gas sampling times needed to obtain a sufficient amount of sampling gas in cases of low pitot pressure were 8 and 12 seconds. The sampling points are indicated in Fig. 3. N_2 was used as an injectant gas. The jet-to-free stream momentum flux ratio J under isentropic assumption was fixed at 1.87 ± 0.07.

Figures 4 (a) and (b) are Schlieren photographs of an injection flowfield without and with probes. As seen here, no remarkable changes in flow structure around the jet are caused by inserting the probes. In addition, no strong interaction between the shock waves from the probes and the boundary layer was observed.

Acetone addition rates

We obtain the rate of acetone addition into the air by reading the fluorescence intensity in a region where the concentration is known. This will be discussed in detail later. Here we will make a rough estimate of the addition rate to consider the effect of acetone addition on the physical properties of air.

The acetone addition rate into the air was estimated in the following way, with the assumption that the acetone molecule is uniformly mixed with air well below the saturated condition. The saturated condition provides the maximum addition rate. The saturated acetone vapor pressure can be calculated by the following equation.[9)]

$$\log_{10}[P_{acetone}(atm)] = 4.244453 - \frac{1214.208}{230.002 + T_{sees}(℃)} \quad (1)$$

Using Eq. (1) and the flow conditions tabulated in Table 1, the saturation acetone addition rate for jet flow at the injector exit condition was estimated at 1.4 %. Since we did not observe any condensation of acetone vapor after injection at any time during the experiment, the seeding rate was less than 1.4 %. For the main flow, the addition rate was estimated to be approximately 0.8 % in the following way. In the bubbling container, acetone was pressurized at 400 kPa and heated to 50 ℃, and the saturated acetone vapor was uniformly mixed into the pressurized air from the air bomb. At this time, the addition rate could be estimated at about 50 %. The acetone/air mixture was then injected into the rectification section and was diluted to 1/60 by inhaled atmospheric air. These addition rates result in an air density change of approximately 1.4 % at most. Therefore, the introduction of this level of acetone seeding has a negligible influence on the estimation of the injectant mole-fraction.

Table 1 Flowfield conditions

	Main	Jet
Total pressure [kPa]	75.0	136.0
Total temperature [K]	291.0	291.0
Static pressure [kPa]	11.0	71.8
Static temperature [K]	168.2	242.5
Flow rate [g/s]	101.1	1.72
Mach number	1.8	1.0

Uncertainty Analysis of experiments

LIF measurement

The total uncertainty inherent in each fluorescence data point, associated with the elements of error sources tabulated in Table 2, is estimated to be approximately 4.1%. For the shot noise, we estimated the uncertainty from the background image. We read out the fluctuation in the main flow region, where the fluorescence is expected to be zero. Variations in the background signals due to laser energy deviation caused a 1.6 % error in the fluorescence reading. The deviations of acetone seeding levels in the jet and main flow were evaluated to be 2.0 % and 2.6 %, from the data for 300 shots. The uncertainty caused by temperature variance is 3 K at most for the whole experimental period. The resulting temperature uncertainty has only a small effect on the fluorescence signal, estimated to be 1.0 %. The uncertainty in the atmospheric temperature and pressure could also affect the values of the absorption cross-section of the acetone molecules, but according to Kashitani et al.[10], the absorption cross-section is almost constant when excited at 266 nm and below the normal pressure range. Therefore, we will neglect the change in the absorption cross-section.

Taking the square root of the sum of the squares of each source yields an overall uncertainty of 4.1 % in the LIF measurement. This number translates directly into a relative fluorescence uncertainty of the same amount, which is consistent in magnitude with the degree of repeatability observed for the same fluorescence experiment repeated at different times.

Table 2 Uncertainty estimates in LIF measurement

Error source	Uncertainty [%]
shot noise	1.6
Deviation of acetone seeding	2.0 (jet) 1.59 (main)
Regulated pressure variance	1.87 (jet) 1.59 (main)
Temperature variance	1.02
Total uncertainty	**4.1 %**

Gas sampling measurement

Errors in the gas sampling measurement are considered to be induced by random uncertainties and systematic error. The random uncertainties were determined by the repeatability for each measurement, resulting in a value of k_{random} = 4.5 %. The systematic error is dominated by deviation in the calibration. We carried out calibration experiments several times and found that there was no day-to-day variation. Therefore, the main factor in the error was the determination process for the best-fitting calibration curve. We obtained the value $k_{systematic}$= 2.0 %, and the overall error was estimated by the following equation.

$$Error_{all} = \sqrt{k_{random}{}^2 + k_{systematic}{}^2} = \underline{4.9\%}$$

Note that, in low pitot pressure regions, such as in the recirculation zone immediately downstream from the injector and near the wall, the error level was relatively large and could reach 10 %.

In summary, there are 4.1 % uncertainties in the LIF measurement and 4.9 % in the gas chromatography.

Generalization of the Fluorescence Ratio Method

The fluorescence intensity S from acetone molecules with broadband absorption spectra is affected by the temperature, pressure, and mole-fraction. It is modeled as Eq. (2) below, assuming linearity in the fluorescence signal, an excitation energy much lower than the saturation energy of the molecules, negligible laser beam attenuation, and negligible radiation trapping.[11-12]

$$S = \eta_{opt} \frac{E}{hc/\lambda} dV_c \sigma(\lambda,T) \phi(\lambda,T,P) \left[\frac{\chi_{acetone} P}{kT} \right] \quad (2)$$

The bracketed term on the right-hand side of Eq. (2) designates the number density of the acetone molecules.

In a compressible flowfield, the thermodynamic state variables of a fluid may vary simultaneously and independently, and it is not possible to get a direct relationship between the LIF signal and the acetone mole-fraction unless there are some additional assumptions.[13]. However, it is clear from Eq. (2) that the fluorescence signal intensity is proportional to the product of the number density of the flow and the mole-fraction of the irradiated fluorescent species.

According to Takahashi et al.[13], the fluorescence signal S can be expressed as a function of the acetone molar concentration $C_{acetone}$ (mol/m^3) in the following form.

$$S = \eta_{opt} \frac{E}{hc/\lambda} \cdot dV_c \cdot \frac{R_{uni}}{k} \cdot \sigma(\lambda,T) \cdot \phi(\lambda,T,P) \cdot C_{acetone} \quad (3)$$

$$C_{acetone} = \frac{\chi_{acetone} \cdot \rho}{m_{acetone}} = N_{acetone} \cdot \frac{k}{R_{uni}} \cdot \frac{m_{mixture}}{m_{acetone}} \quad (4)$$

Note that the estimated maximum error of ± 6 % over the entire flowfield is included when converting the fluorescence signal to molar concentration with calculated conditions of 0.1 atm ≤ P ≤ 1 atm for pressure, 100 K ≤ T ≤ 300 K for temperature, and 0 % ≤ χ ≤ 100 % for acetone mole-fraction.

—When only the injectant jet is seeded with acetone, the fluorescence signal is proportional to the number density of the acetone fed by the jet. When both the jet and the main flow are seeded, the fluorescence signal is proportional to the sum of the acetone number densities fed by the jet and the main flow. These cases are illustrated as a simplified model in Fig. 5. If the acetone is uniformly mixed in both the jet and the main flow, the acetone number density is related to the total number density of the seeded source by

$$\chi_{ac\_j} N_j = \chi_{ac\_j} \chi_j N_{total}$$
$$\chi_{ac\_m} N_m = \chi_{ac\_m} (1-\chi_j) N_{total} \quad (5)$$

If the same laser sheet and optical-collection geometries are used in both measurements, the laser sheet intensity variation is canceled as well. Taking these facts into account and using Eqs. (3) to (5), the acetone fluorescence signal is expressed as follows.

In the case of jet-only seeding (case 1),

$$S_1 \propto \chi_{ac\_j1} N_j m_j = \chi_{ac\_j1} \chi_j m_j N_{total} \quad (6)$$

In the case of entire-flow seeding (case 2),

$$S_2 \propto \chi_{ac\_j2} N_j m_j + \chi_{ac\_m2} N_m m_m = \left\{ \chi_{ac\_j2} \chi_j m_j + \chi_{ac\_m2} (1-\chi_j) m_m \right\} N_{total} \quad (7)$$

Dividing the image acquired in case 1 by the one in case 2, the resulting ratio of fluorescence signals is related to the injectant mole-fraction by the following equation:

$$\frac{S_1}{S_2} = \frac{\chi_{ac\_j1} \chi_j m_j}{\chi_{ac\_j2} \chi_j m_j + \chi_{ac\_m2} (1-\chi_j) m_m} \quad (8)$$

Rearranging this equation, we get an explicit equation for the injectant mole-fraction.

$$\chi_j = \frac{\left(\frac{\chi_{ac\_m2}}{\chi_{ac\_j2}}\right)\left(\frac{m_m}{m_j}\right)}{\left(\frac{\chi_{ac\_m2}}{\chi_{ac\_j2}} \cdot \frac{m_m}{m_j} - 1\right) + \left(\frac{S_2}{S_1}\right)\left(\frac{\chi_{ac\_j1}}{\chi_{ac\_j2}}\right)} \quad (9)$$

The value of $\chi_{ac\_j1}/\chi_{ac\_j2}$ is a constant used to adjust for the slight difference in the acetone seeding rates into the jet for the two cases. The value of $\chi_{ac\_m2}/\chi_{ac\_j2}$ is determined in the following way. In this study, we deal with only gas flows so that the ratio of the seeding rates of the jet and main flow is equal to the ratio of the mole-fractions of acetone in the two flows.

Taking these facts into account and using Eqs. (3) and (4), we can obtain the following relationship.

$$\left(\frac{\chi_{ac\_m2}}{\chi_{ac\_j2}}\right)\left(\frac{m_m}{m_j}\right) = \left[\left(\frac{S_j}{S_m}\right)\left(\frac{\rho_m}{\rho_j}\right)\right]_{ref} \quad (10)$$

The right-hand side of Eq. (10) is the reference value. The fluorescence intensities S_j and S_m at the reference points are read from the PLIF image in case 2. S_j is the intensity at the injector orifice, and S_m is the intensity at the main flow region in front of the bow shock wave. The values of ρ_j and ρ_m at the reference points will be derived from the respective stagnation conditions and isentropic relationships for the injection orifice and the inlet of the test section.

As mentioned previously, the change in molecular weight due to acetone seeding is negligible in the present experiment, hence,

$$\frac{m_j}{m_m} \approx 1 \quad (11)$$

Finally, we obtain the following relationship with regard to the acetone seeding ratio.

$$\frac{\chi_{ac\_m2}}{\chi_{ac\_j2}} \approx \left[\left(\frac{S_j}{S_m}\right) \cdot \left(\frac{\rho_m}{\rho_j}\right)\right]_{ref} \quad (12)$$

Using Eqs. (9) and (12), we can then obtain the injectant mole-fraction distribution.

—From Eq. (9), it is obvious that the value of χ_{jet} varies with $\chi_{ac\_m2}/\chi_{ac\_j2}$ as well as with S_2/S_1. Figure 6 plots the dependence of injectant mole-fraction χ_{jet} on $\chi_{ac\_m2}/\chi_{ac\_j2}$. As we can clearly observe, the value of χ_{jet} for a given S_2/S_1 largely varies with $\chi_{ac\_m2}/\chi_{ac\_j2}$.

The Hartfield method, expressed in Eq. (13), corresponds to a special case where $\chi_{ac\_m2}/\chi_{ac\_j2}$ equals unity.

$$\chi_j = \frac{\chi_{ac\_j2}}{\chi_{ac\_j1}} \cdot \frac{S_1}{S_2} \quad (13)$$

For $\chi_{ac\_m2}/\chi_{ac\_j2}$ other than unity, we need to use Eq. (9) to obtain the injectant mole-fraction distribution from the PLIF data.

Results and Discussion

Verification of acetone seeding uniformity

The fluorescence fluctuations were measured to quantify the uniformity of the flow and acetone seeding in the main stream. The spatial fluctuation intensity of the fluorescence signal was measured on a line across the exit of the Laval nozzle. The level of fluctuation was on the order of 2 %. Since this

fluctuation was mainly caused by variations in the acetone addition rate, the level of fluctuation agrees well with the error estimated from the acetone addition rate and the uncertainty analysis. This results in a 2 % level of characteristic fluctuation in the jet-to-freestream momentum flux ratio due to the change in molecular weight of the main stream, an acceptable level for the present experiment.

Flow visualization by acetone PLIF

Figures 7 (a) and (b) are mean fluorescence images obtained from 300 instantaneous frames in the center plane of the test section for the jet-only and entire seeding conditions. In each image, background scattered noise was subtracted and the non-uniformity of the laser sheet intensity was corrected. The flowfield near the opposite wall was masked in the image because of strong noise due to reflection of the laser sheet from the wall. In the image for jet-only seeding, the fluorescence signal varies with changes in both the injectant mole-fraction and the local density. In Fig. 7 (b) for the entire seeding, the strong density dependence of the fluorescence signal is evident in the large variation in signal intensity across the bow shock wave generated by injection. These figures represent the distributions of acetone molar concentration.

Figure 8 (a) depicts the ratio of the images in Fig. 7 (a) and Fig. 7 (b) with the value of $\chi_{ac\_j1}/\chi_{ac\_j2}$ in Eq. (13), determined by the intensity at the injection port of the jet for each image. If we were to adopt the Hartfield model, this image would directly represent the injectant mole-fraction distribution. In this study, the value of $\chi_{ac\_m2}/\chi_{ac\_j2}$ determined from the results of five independent experiments was not unity but rather was 0.50 $\pm$0.10. Hence the distribution described in Fig. 8 (a) represents not the quantitatively correct mole-fraction distribution, but a qualitative one.

The injectant mole-fraction distribution obtained from the images of Figs. 7 (a) and 7 (b) using Eqs. (9) and (10) is shown in Fig. 8 (b). The difference between Fig. 8 (a) and Fig. 8 (b) is not very clear because the value of $\chi_{ac\_m2}/\chi_{ac\_j2}$ in the present experiment was not very far from unity. We will discuss the difference in more detail later with some cross-sectional profiles, and will compare them with gas sampling data.

Figure 9 shows cross-sectional mole-fraction distributions at five streamwise locations (x/D = 0, 4, 8, 12, and 16). When these cross-sectional images were acquired, the photograph was taken by a camera set to 45 degrees against the cross section. The inclined images were corrected to plan-view images in post-processing.

The cross-sectional distributions indicate that a core region of jet where no mixing occurred remained for x/D = 0 and 4. The plume of injectant became a distinctive horseshoe shape in the downstream region and was completely lifted up from the wall by the section of x/D = 4. Splitting or bifurcation of the jet core is seen to occur by x/D = 8. The horseshoe shape and the lifting and bifurcation of the jet plume are due to a pair of strong counter-rotating streamwise vortices generated downstream of the jet.

Comparison of PLIF and gas chromatography

Figure 10 presents a comparison of PLIF and gas chromatography data for the mole-fraction profiles at x/D = 4 and 8 in the center plane. Since the injector diameters were not the same in the two experiments, the comparison was made at the same non-dimensional distance from the injector normalized by each jet diameter. In Fig. 10, the dashed line represents the PLIF data processed with the Hartfield method, the solid line represents data processed with the generalized method developed in this paper, and the square symbols represent the gas sampling data.

The gas sampling data shows better agreement with the generalized PLIF line than with the Hartfield line. Figure 11 is a combined plot of the gas sampling data profiles at x/D = 2, 4, 6, 8, 10, and 12, along with the generalized PLIF distribution. We can see that the generalized PLIF profiles and the gas sampling data agree well over the entire region except for the portion near the bottom wall, where we observed large systematic errors in the PLIF due to light scattered by the wall and errors in the gas sampling due to the extremely low pitot pressure.

As the final step in this study, we made an overall comparison of the mole-fractions obtained from the PLIF data and from the gas sampling data. The result appears in Fig. 12. The solid black line with an angle of 45 degrees is the ideal case, in which the PLIF data and the gas sampling data agree perfectly. The open and solid symbols were calculated with the Hartfield method and the present generalized method. The circular and square symbols correspond to $\chi_{ac\_m2}/\chi_{ac\_j2}$ = 0.5 and 0.3. The error bars were determined by the uncertainty analysis, namely, 4.9 % for the gas sampling data and 4.1 % for the PLIF data, with both kinds of processing. Theoretical curves for the Hartfield method with $\chi_{ac\_m2}/\chi_{ac\_j2}$ = 0.5 and 0.3 calculated from Eq. (8) are also plotted in the figure. From the graph, we can clearly see that the mole-fraction data obtained with the Hartfield method tends to distribute around the theoretical curves for the corresponding values of $\chi_{ac\_m2}/\chi_{ac\_j2}$. In contrast, the present generalized method resulted in better agreement with the ideal line irrespective of the value of $\chi_{ac\_m2}/\chi_{ac\_j2}$. Although the unevenness of the generalized data points around the ideal line is relatively large, the generalized fluorescence ratio method presented in this paper derives quantitatively correct mole-fractions from the PLIF data.

Concluding remarks

A generalization of Hartfield's fluorescence ratio method was extended for different seeding rates of fluorescent molecules to the jet and the main stream. The generalized method was validated by a comparison with gas sampling data. The comparison revealed that the mole fractions obtained with the generalized method agree better with the gas sampling data than do those obtained with Hartfield's original method.

Acknowledgements

The authors express their gratitude to Shuya Shida for his assistance in the experiment.

References

1) Gutmark, E. J., Schadow, K. C., and Yu, K. H.: Mixing Enhancement in Supersonic Free Shear Flows, *Annual Review of Fluid Mechanics*, **27**, 1995, pp. 375-417
2) Lozano, A., Yip, B., and Hanson, R. K.: Acetone: A Tracer for Concentration Measurements in Gaseous Flows by Planar Laser- Induced Fluorescence, *Experiments in Fluids* **13**, 1992, pp. 369-379.
3) Abbitt Ⅲ, J. D., Hartfield, R. J., and McDaniel, J. C.: Mole-Fraction Imaging of Transverse Injection in a Ducted Supersonic Flow, *AIAA Journal*, **29** (3), 1991, pp.431-435
4) Hartfield Jr., R. J., Abbitt Ⅲ, J. D., and McDaniel, J.C.: Injectant mole-fraction imaging in compressible mixing flow using planar laser-induced iodine fluorescence, *Optics Letters*, **1** (16), 1989, pp.850-852
5) Hartfield Jr., R. J., Abbitt Ⅲ, J. D., and McDaniel, J.C.: Mixing from a Slot Injector in Compressible Flow with an Adverse Pressure Gradient, AIAA-95-0521, 1995
6) Donohue, J. M., McDaniel Jr., J. C., Haj-Hari, H.: Experimental and Numerical Study of Swept Ramp Injection into a Supersonic Flowfield, *Journal of Propulsion and Power*, **32** (9), 1994, pp. 1860-1867
7) Hollo, S. D., McDaniel, J. C., Hartfield Jr., R. J.: Quantitative Investigation of Compressible Mixing: Staged Transverse Injection into Mach 2 Flow, *Journal of Propulsion and Power*, **32** (3), 1994, pp. 528-534
8) Hartfield Jr., R. J., Hollo, S. D., McDaniel, J. C.: Experimental Investigation of a Supersonic Swept Ramp Injector Using Laser-Induced Iodine Fluorescence, *Journal of Propulsion and Power*, **10** (1), 1994, pp. 129-135
9) Yuen, L. S., Peters, J. E., and Lucht, R. P.: Pressure Dependence of Laser-induced Fluorescence from Acetone, *Applied Optics*, **36** (15), 1997, pp. 3271-3277
10) Kashitani, M., Yamaguchi, Y., Handa, T., Masuda, M., Matsuo, K.: A Preliminary Study on Acetone Laser-Induced Fluorescence Technique for Low Temperature Flows, AIAA Paper, 2004-385, 2004
11) Koch, J.: Fuel Tracer Photophysics for Quantitative Planar Laser-Induced Fluorescence, Ph.D dissertation, Department of Mechanical Engineering, Stanford University, 2005
12) Thurber, M. C.: Acetone Laser-Induced Fluorescence for Temperature and Multi parameter Imaging in Gaseous Flows, Ph.D dissertation, Department of Mechanical Engineering, Stanford University, 1999
13) Takahashi, H., Hirota, M., Oso, H., and Masuya, G. : Measurement of Supersonic Flowfield using Acetone PLIF, *Journal of JSASS*, **55** (642), 2007, pp.318-323, (in Japanese)

Nomenclature

c	=	velocity of light [m/s]
dV_c	=	optical collection volume [cm^3]
D	=	diameter of injector [m]
E	=	laser fluence [J/cm^2]
f	=	mole-fraction of injectant
h	=	Planck's constant [J·s]
J	=	jet-to-freestream momentum flux ratio
k	=	Boltzmann constant [J/K]
M	=	Mach number
m	=	molecular weight [kg/mol]
N	=	number density [cm^{-3}]
P	=	local pressure [Pa]
R	=	gas constant [J/(K·mol)]
S	=	fluorescence signal intensity
T	=	local temperature [K]
u	=	velocity [m/s]
η_{opt}	=	overall efficiency of collection optics
σ	=	molecular absorption cross-section of excited molecules [cm^2]
ϕ	=	fluorescence quantum yield of acetone
λ	=	excitation wavelength of laser [nm]
χ	=	mole-fraction
ρ	=	density [kg/m^3]

Subscripts

acetone	=	component of acetone
ac_j	=	acetone seeding in jet
ac_m	=	acetone seeding in main flow
exit	=	flow condition at jet exit
j	=	jet
m	=	main flow
mixture	=	acetone/air mixture gas
ref	=	reference condition
total	=	jet and main flow
uni	=	universal
1	=	acetone seeding only in jet
2	=	acetone seeding in both jet and main flow

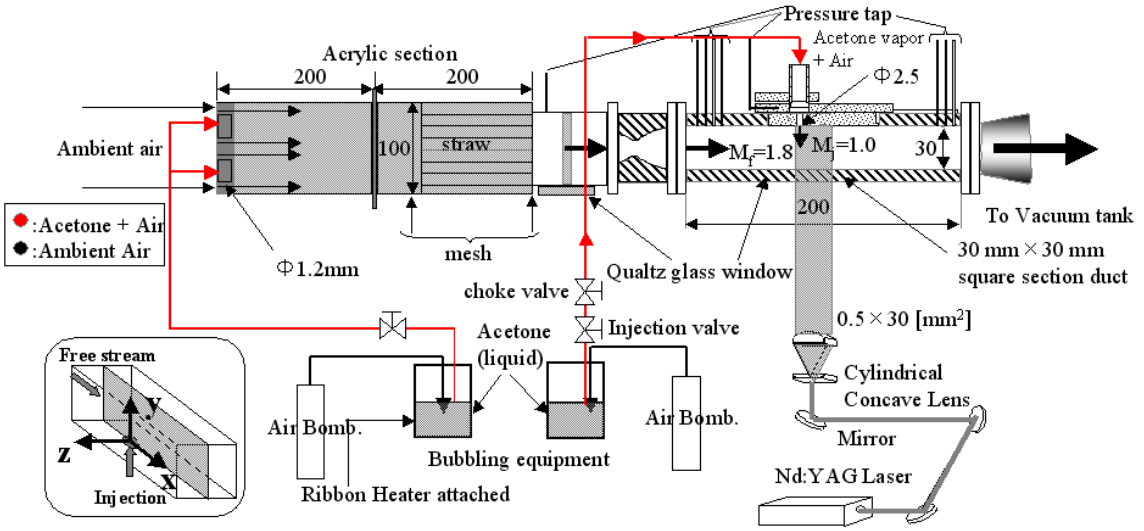

Fig. 1 Schematic diagram of the test facility

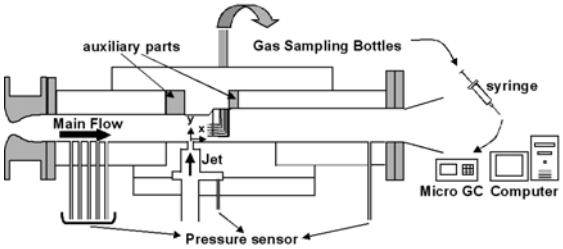

Fig. 2 Test section for gas sampling

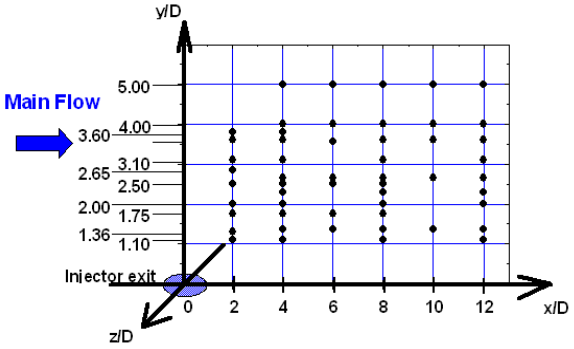

Fig. 3 Sketch of the measurement points for gas sampling

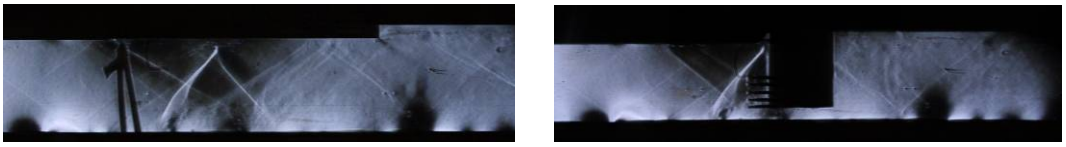

(a) Without probes (b) With probes

Fig. 4 States of the flowfield pictured by Schlieren photographs in case of gas sampling
(Main flow direction is from left to right.)

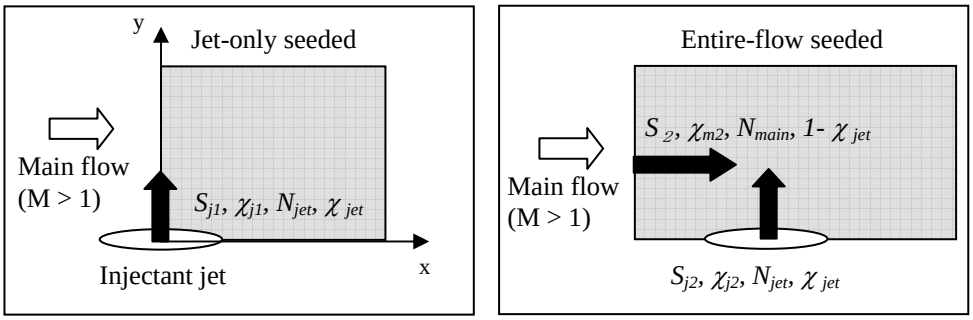

Fig. 5 Schematic diagram of a simplified model of acetone seeding methods in a flowfield of interest

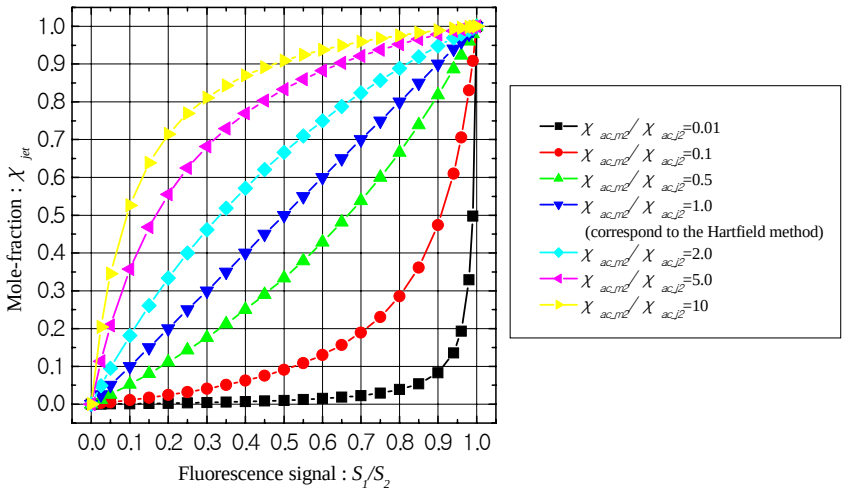

Fig. 6 Variation in mole-fraction against fluorescence signal with the change of $\chi_{ac\_m2}/\chi_{ac\_j2}$

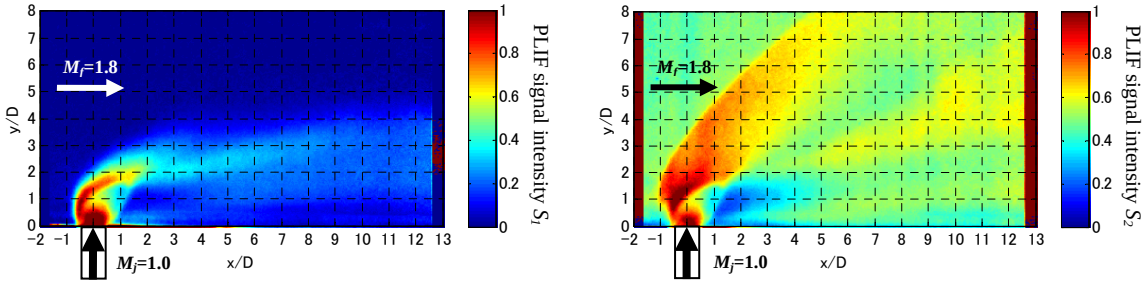

(a) Jet-only seeded image (case 1) (b) Entire flowfield seeded image (case 2)

Fig. 7 Mean images of acetone PLIF in the center plane

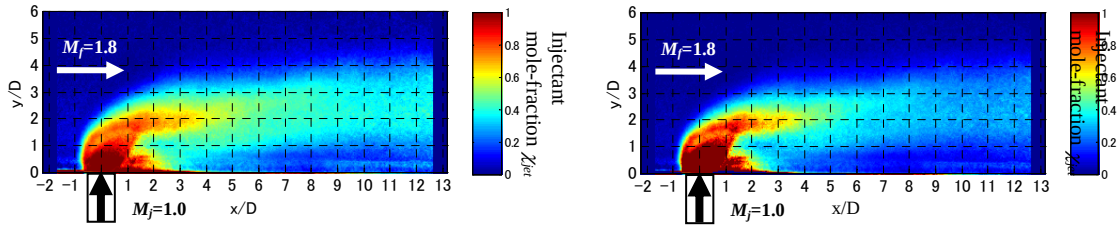

(a) Based on the Hartfield method (b) Based on the present method

Fig. 8 Injectant mole-fraction distribution in the center plane obtained by two fluorescence ratio methods

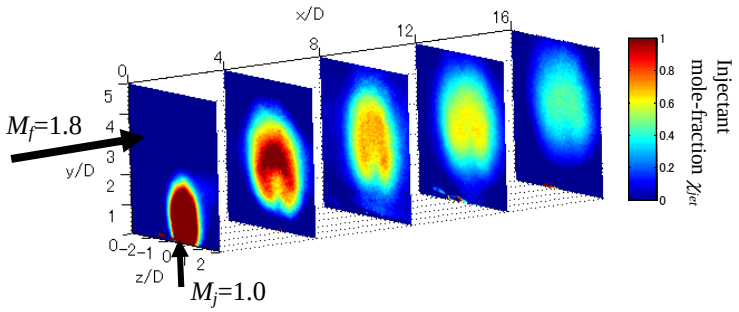

Fig. 9 Injectant mole-fraction distributions in cross-sectional planes

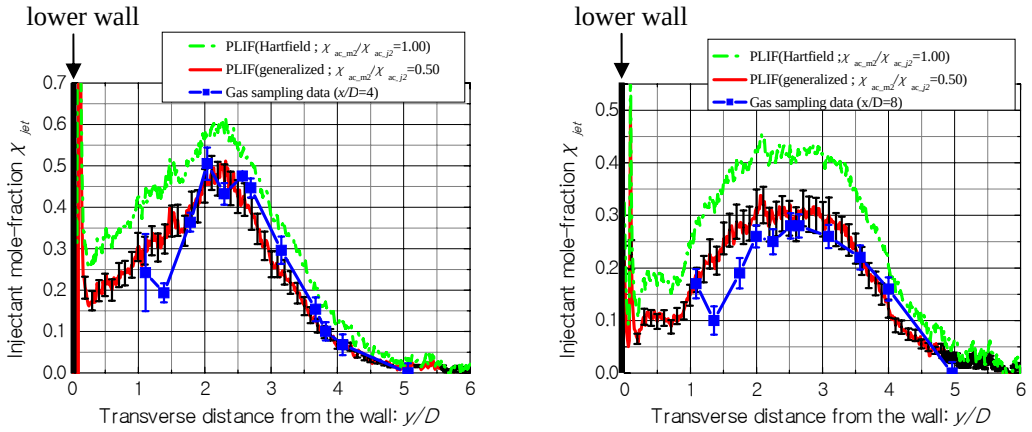

(a) Mole-fraction profiles at x/D = 4 (b) Mole-fraction profiles at x/D = 8

Fig. 10 Comparison of PLIF and gas chromatography for mole-fraction profiles of x/D = 4 and 8

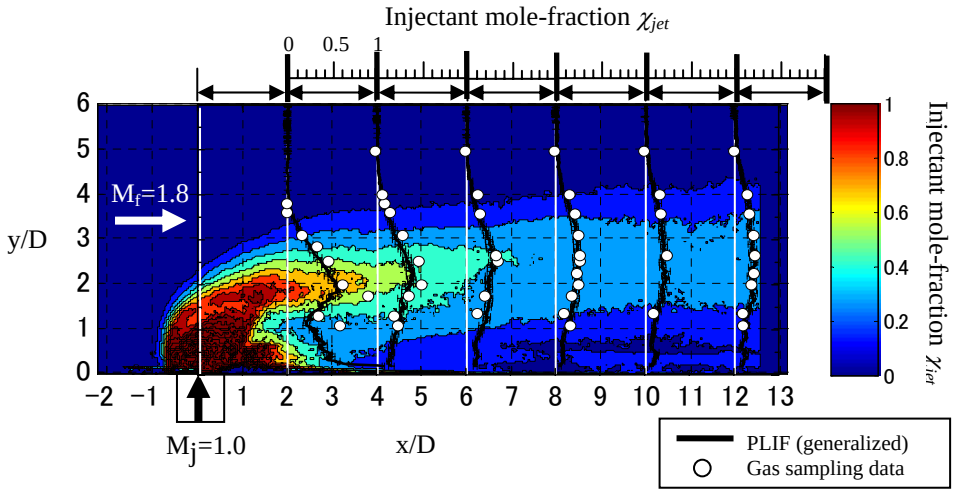

Fig. 11 Comparison of PLIF and gas chromatography

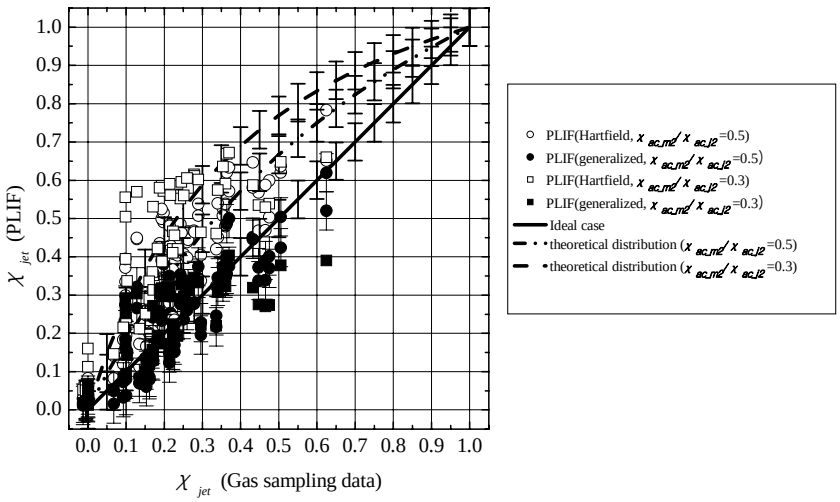

Fig. 12 Comparison of mole-fraction value between PLIF and gas chromatography